Quasi-ballistic thermal transport in $Al_{0.1}Ga_{0.9}N$ thin film semiconductors

Yee Rui Koh, MohammadAli Shirazi-HD, Bjorn Vermeersch, Amr M. S. Mohammed, Jiayi Shao, Gilles Pernot, Je-Hyeong Bahk, Michael J. Manfra, and Ali Shakouri

Citation: Appl. Phys. Lett. **109**, 243107 (2016); doi: 10.1063/1.4972186
View online: http://dx.doi.org/10.1063/1.4972186
View Table of Contents: http://aip.scitation.org/toc/apl/109/24
Published by the American Institute of Physics

Quasi-ballistic thermal transport in $Al_{0.1}Ga_{0.9}N$ thin film semiconductors

Yee Rui Koh,[1,2,a),b)] MohammadAli Shirazi-HD,[1,2,a)] Bjorn Vermeersch,[3] Amr M. S. Mohammed,[1,2] Jiayi Shao,[2] Gilles Pernot,[4] Je-Hyeong Bahk,[5] Michael J. Manfra,[1,2,6,7] and Ali Shakouri[1,2,c)]

[1]*School of Electrical and Computer Engineering, Purdue University, West Lafayette, Indiana 47907, USA*
[2]*Birck Nanotechnology Center, Purdue University, West Lafayette, Indiana 47907, USA*
[3]*CEA-LITEN, 17 Rue des Martyrs, Grenoble 38054, France*
[4]*Université de Lorraine, LEMTA, UMR7563, CNRS, F-54506 Vandoeuvre Les Nancy, France*
[5]*Department of Mechanical and Materials Engineering, University of Cincinnati, Cincinnati, Ohio 45221, USA*
[6]*School of Materials Engineering, Purdue University, West Lafayette, Indiana 47907, USA*
[7]*Department of Physics and Astronomy, Purdue University, West Lafayette, Indiana 47907, USA*

(Received 27 July 2016; accepted 1 December 2016; published online 16 December 2016)

We investigate thermal transport in high-quality $Al_{0.1}Ga_{0.9}N$ thin films grown using plasma-assisted molecular beam epitaxy by time-domain thermoreflectance (TDTR) in the 100 K–500 K temperature range. The apparent thermal conductivity at 300 K and 500 K drops by 30% when the laser modulation frequency is increased from 0.8 MHz to 10 MHz. Tempered Lévy analysis of the quasi-ballistic heat conduction reveals superdiffusion exponents $\alpha \approx 1.70 \pm 0.06$ at room temperature and $\alpha \approx 1.83 \pm 0.16$ at 500 K. We describe limitations in concurrent extraction of other model parameters and also discuss the impact of boundary scattering in the 100 K–200 K temperature range. *Published by AIP Publishing.* [http://dx.doi.org/10.1063/1.4972186]

III–V nitride semiconductors have a wide and direct bandgap favorable for high power and high frequency electronic and optoelectronic applications. Among the possible alloys of GaN, $Al_xGa_{1-x}N$ is widely used in high electron mobility transistors and light emitting diodes (LEDs). Control of the device temperature is critical for the performance and also long-term reliability of these devices. Therefore, temperature-dependent and frequency-dependent thermal transport in GaN and $Al_xGa_{1-x}N$ films are important in high power or high frequency applications.[1]

The thermal conductivity of $Al_xGa_{1-x}N$ thin films was first reported by Daly *et al.*[2] for $Al_{0.18}Ga_{0.82}N$, $Al_{0.2}Ga_{0.8}N$, and $Al_{0.44}Ga_{0.56}N$, giving values of ~14 W/mK, ~13.5 W/mK, and ~6.5 W/mK, respectively, at 300 K without specifying the sample thicknesses. An early theoretical paper on bulk thermal conductivity of $Al_xGa_{1-x}N$ using a simplified model of alloy-disorder scattering was reported by Adachi *et al.*,[3] which is in agreement with Refs. 4 and 5. However, the measurement results reported by Daly *et al.* for $Al_{0.44}Ga_{0.56}N$ are much lower compared to the theoretical predictions of Refs. 3–5. We suspect that this discrepancy may be due to the small thicknesses of the $Al_{0.44}Ga_{0.56}N$ layer.

In the present article, thermal conductivity of a relatively thick 1.2 μm high quality $Al_{0.1}Ga_{0.9}N$ thin film is measured using time-domain thermoreflectance (TDTR) over the frequency range $0.8 < f < 10$ MHz and temperature range $100 < T < 500$ K. The measured thermal conductivity at low pump modulation frequency (0.8 MHz) agrees with results by Adachi *et al*. This indicates that the film thickness is large enough to extract the bulk thermal conductivity of $Al_{0.1}Ga_{0.9}N$.

Interestingly, the apparent thermal conductivity of $Al_{0.1}Ga_{0.9}N$ is reduced by 30% when the laser modulation frequency increases from 0.8 to 10 MHz at 300 K. This frequency dependence resembles prior observations by Koh and Cahill on other alloys[6] and is an indication of quasi-ballistic heat transport, which has generated extensive experimental and theoretical work. At distances comparable to phonon MFPs, thermal transport in semiconductor alloys no longer obeys Brownian motion but is instead governed by Lévy superdiffusion with fractal dimension, α.[7–9] The fractal dimension is also known as the superdiffusion exponent. Here, both conventional Fourier diffusion and Lévy superdiffusion are used to analyze $Al_xGa_{1-x}N$ TDTR data. The temperature-dependent apparent thermal conductivity has a peak at relatively high temperatures, $T \sim 300$ K. This helps to study the impact of different phonon scattering mechanisms such as boundary and Umklapp scattering at low temperatures (100 K and 200 K). Quasi ballistic thermal transport can impact the transient temperature response of power devices[7] and understanding of different phonon scattering mechanisms can be used to improve the thermal management of sub-micron $Al_xGa_{1-x}N$ devices.

The samples were grown by plasma-assisted molecular beam epitaxy (PAMBE) on commercially available 3.5 μm thick semi-insulating (0001) GaN templates on sapphire. The radio-frequency plasma source was set to 300 W with 0.5 SCCM of nitrogen flow corresponding to a growth rate of 7 nm/min for GaN. The samples consist of a 150 nm thick GaN buffer followed by the $Al_xGa_{1-x}N$ layer grown under Ga-rich conditions at a substrate temperature of 720 °C measured by optical pyrometry. The excess gallium acts as a surfactant to ensure smooth morphology and to suppress formation of cracks due to the lattice mismatch at the GaN/$Al_xGa_{1-x}N$ interface. A constant Ga beam flux was used

a)Y. R. Koh and M. A. Shirazi equally contributed to this work.
b)koh7@purdue.edu
c)shakouri@purdue.edu

during the entire growth with an Al beam flux corresponding to an $Al_xGa_{1-x}N$ layer with ~10% Al composition. 0.2 μm and 1.2 μm thick $Al_{0.1}Ga_{0.9}N$ layers were grown without growth interruptions. A GaN cap layer developed on the $Al_{0.1}Ga_{0.9}N$ films stemming from the continued growth of the accumulated gallium at the end of $Al_{0.1}Ga_{0.9}N$ layer.

The surface morphology of the $Al_{0.1}Ga_{0.9}N$ samples was characterized using atomic force microscopy (AFM). As depicted in Figure 1(a) and 1(b), both samples have smooth morphologies with root-mean-square (rms) roughness less than 0.5 nm over a 1 μm × 1 μm area. Despite the Ga-rich growth, no Ga droplets were observed on the surface. However, due to accumulated tensile strain in the epitaxial $Al_xGa_{1-x}N$ layer, a low density of cracks was observed on the 1.2 μm thick $Al_{0.1}Ga_{0.9}N$ sample, which suggests a low degree of relaxation. The Al composition and thickness of the $Al_{0.1}Ga_{0.9}N$ layers were verified by high-resolution x-ray diffraction (HRXRD) using a symmetric ω-2Θ scan around the (0002) GaN reflection using Cu Kα1 radiation in a PANalytical X'pert Pro *Materials Research Diffractometers (*MRD). The ω-peak separation between $Al_{0.1}Ga_{0.9}N$ and GaN revealed an Al composition of 9.1% for both samples. The $Al_xGa_{1-x}N$ layer thickness was extracted from the thin film interference in the ω-2Θ scan, confirming 0.2 μm and a 7 nm/min growth rate for the first sample. Using similar growth conditions, the second sample was grown for a longer duration to get a 1.2 μm AlGaN film. Figure 1(c) shows the ω-2Θ HRXRD overlay of the 0.2 μm and 1.2 μm thick $Al_{0.1}Ga_{0.9}N$ samples.

The TDTR technique was used to characterize the thermal conductivity of $Al_{0.1}Ga_{0.9}N$ thin films.[10–12] A Ti:Sapphire femtosecond laser creates 150 fs short pulse laser beams with a wavelength of 780 nm and a repetition rate of ~12.5 ns.[13] The laser pulses were split into a pump beam and a probe beam. The pump beam has a higher power to heat up the sample surface and is modulated at a frequency of 0.8–10 MHz. The radii of the laser beams are ~5.5 μm at the surface of the sample. A 70 nm aluminum transducer was deposited on the sample to effectively absorb the incident pump beam. The optical absorption of the transducer has been reported in Refs. 14 and 15 Optical transmission into the thin film is small and can be neglected. The probe laser has a lower power. The reflected probe beam signal from the sample surface was collected by a Si-photodetector and a RF lock-in amplifier. The increase of the sample surface temperature during the measurements was limited to ~10 °C by using suitable laser power. The obtained probe beam signal that is a function of the transient surface temperature was fitted with a 3D thermal diffusion model based on thermal quadrupoles (see supplementary material).[10,16] The interface resistance between the Al transducer and $Al_{0.1}Ga_{0.9}N$ thin film was included in the model. The precision of the thermal conductivity measurements is approximately ±5–10%.[17] The sample was placed in the LINKAM THMS600 chamber, which allows precise temperature control down to ±0.1 °C. A nitrogen gas purge of the chamber was done before the TDTR measurement in order to remove air and minimize condensation on the sample surface.

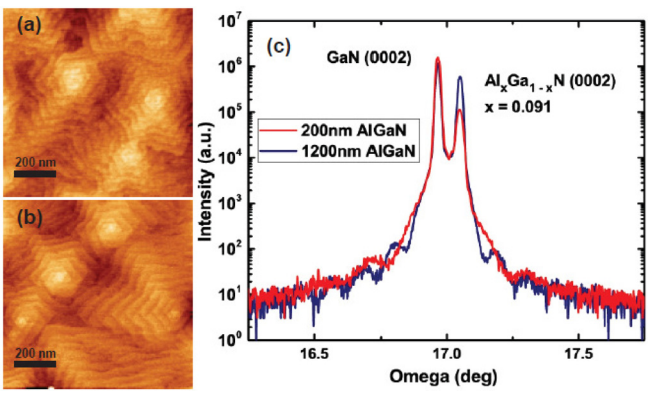

FIG. 1. (a) 1 μm × 1 μm AFM images of 0.2 μm thick and (b) 1.2 μm thick AlGaN samples. The Z scale of the AFM images is 3.4 nm. The rms roughness of the AFM images is 0.43 nm. The surface morphology displays spiral hillocks around mixed dislocations, characteristic of MBE growth of $Al_xGa_{1-x}N$. (c) HRXRD ω-2Θ scans of AlGaN samples around the (0002) GaN reflection. The $Al_xGa_{1-x}N$ molar fraction x = 0.091 is determined from the peak separation. Largely spaced fringes on the HRXRD measurements indicate the presence of 25 nm and 40 nm GaN cap layers on top of the 0.2 μm and 1.2 μm AlGaN films, respectively, resultant of excess gallium on the surface at the end of the growth.

In addition to conventional effective thermal conductivity extraction, we also analyze the measurement results with a Tempered Lévy model.[18] This quasi-ballistic framework is an extension of previous Truncated Lévy analyses[7–9] that offer a rigorous treatment of 3D heat spreading with superior computational performance. The transport of thermal energy is modeled as a stochastic process having Fourier-space single pulse response $P(\vec{\xi},t) = \exp[-\psi(\|\vec{\xi}\|)t]$, where $\vec{\xi}$ is the spatial Fourier variable and t is the time. The propagator is given by $\psi(\|\vec{\xi}\|) = D\|\vec{\xi}\|^2/(1 + r_{LF}{}^2\|\vec{\xi}\|^2)^{1-\alpha/2}$. This describes a transition, over characteristic length scale r_{LF}, from Lévy superdiffusion $\psi(\|\vec{\xi}\|) = D_\alpha\|\vec{\xi}\|^\alpha$ with fractal dimension α and fractional diffusivity $D_\alpha = D/r_{LF}{}^{2-\alpha}$ (unit $m^{\alpha/s}$) to regular Fourier diffusion (Brownian motion) with nominal diffusivity D. The single pulse thermal response is then convolved based on the laser repetition rate and the external modulation frequency to fit the TDTR data. Lévy dynamics arise naturally in semiconductor alloys due to mass impurity phonon scattering and are responsible for the frequency dependence of apparent conductivity.[8] By properly accounting for phonons with long mean-free-paths and the quasi-ballistic transport, Lévy models enable more accurate determination of transient temperature distribution inside the semiconductor and the inherent metal/semiconductor thermal interface resistance.[9] The framework has also been used to investigate thermal transport in alloys as a function of embedded nanoparticle concentration.[19] It was shown that the Lévy fractal dimension is invariant when nanoparticle concentration increases by two orders of magnitude and thermal conductivity is reduced by a factor of 3.

Figure 2 shows the thermal conductivity of $Al_xGa_{1-x}N$ versus the aluminum content in the alloy samples. The measurement results of $Al_{0.1}Ga_{0.9}N$ thermal conductivity are compared to Refs. 2, 20, and 21 for $Al_xGa_{1-x}N$ samples with different Al contents at 300 K. References 20 and 21 used the 3ω technique to measure the 700 nm thick thin film, while Ref. 2 employed the pump and probe TDTR method. We employed a pump modulation frequency of 0.8 MHz for the 1.2 μm sample to extract the bulk thermal conductivity of the $Al_{0.1}Ga_{0.9}N$ alloy. The Fourier thermal penetration depth (~1.8 μm) for the 0.8 MHz modulation frequency is greater

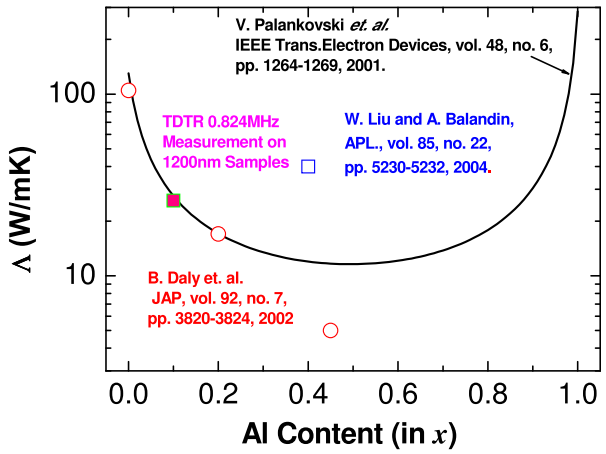

FIG. 2. Thermal conductivity of the $Al_xGa_{1-x}N$ versus aluminum percentage. The black solid line indicated the theoretical calculation of Ref. 5. Open circles and squares indicate the thermal conductivity measurement results.

than the sample thickness (1.2 μm). The thermal penetration depth is defined as $d = \sqrt{\Lambda/(\pi C f)}$, where Λ is the thermal conductivity, C is the heat capacity per unit volume, and f is the modulation frequency. The large penetration depth is sufficient to probe the majority of phonons that contribute to the thermal conductivity. The measured thermal conductivity of the $Al_{0.1}Ga_{0.9}N$ alloy is ~24.5 W/mK at 300 K, which is in agreement with those in Refs. 3–5.

Thermal conductivity as a function of temperature for $Al_{0.1}Ga_{0.9}N$ as well as $Al_{0.18}Ga_{0.82}N$, $Al_{0.2}Ga_{0.8}N$, and $Al_{0.44}Ga_{0.56}N$[2] is shown in Figure 3. The alloy thermal conductivity at low temperatures increases and follows the temperature dependence of the specific heat capacity ($c_v \sim T^3$) until the maximum thermal conductivity is reached. At higher temperatures, the thermal conductivity is dominated by the Umklapp scattering.[22] Figure 3 shows how the peak thermal conductivity changes for $Al_xGa_{1-x}N$ samples with different Al contents. $Al_{0.1}Ga_{0.9}N$, $Al_{0.18}Ga_{0.82}N$, $Al_{0.2}Ga_{0.8}N$, and $Al_{0.44}Ga_{0.56}N$ have the maximum thermal conductivity at 300, 225, 200, and 150 K, respectively. The extracted temperature dependence of the thermal conductivity for $Al_{0.1}Ga_{0.9}N$ approximately follows $T^{-0.35}$ in 300–500 K temperature range. This value is comparable to Daly *et al.* measurements of $Al_xGa_{1-x}N$ samples ($T^{-0.4}$–$T^{-0.5}$) and the theoretical prediction of Klemens ($T^{-0.5}$).[23,24]

In order to observe the frequency-dependent thermal conductivity in $Al_xGa_{1-x}N$ samples, the Al fraction should be high enough to reduce the contribution of high-frequency phonons by alloy scattering. However, low-x $Al_xGa_{1-x}N$ films are preferred to avoid macroscopic cracks and defects in thick epi-layers due to the lattice-mismatch between high-x $Al_xGa_{1-x}N$ and the GaN substrate. Therefore, we examined a 1.2 μm thick $Al_xGa_{1-x}N$ sample with x = 0.1 in this study. Figure 4 shows the apparent thermal conductivity versus the pump modulation frequency of the $Al_{0.1}Ga_{0.9}N$ samples at 100–500 K temperature range. The apparent thermal conductivity of the 1.2 μm thick $Al_{0.1}Ga_{0.9}N$ drops from 24.5 W/mK to 18 W/mK as the modulation frequency increases from 0.8 to 10 MHz at room temperature. For the 0.2 μm thick $Al_{0.1}Ga_{0.9}N$, the modulation frequencies were carefully selected so the penetration depth would match the sample thickness. Both thermal conductivities of the 1.2 and 0.2 μm thick $Al_{0.1}Ga_{0.9}N$ are close at 6.5 and 10 MHz at room temperature. The consistent thermal conductivity in 1.2 μm and 0.2 μm thick $Al_{0.1}Ga_{0.9}N$ proves that the reduction of the thermal conductivity in the 1.2 μm thick $Al_{0.1}Ga_{0.9}N$ is not due to defects in the samples. The higher heat penetration depth in the 1.2 μm sample causes slightly higher thermal conductivity in the 1.2 μm sample compared to the 0.2 μm sample at 6.5 and 10 MHz. Thermal conductivity of $Al_{0.1}Ga_{0.9}N$ decreases with increasing the modulation frequency at 300–500 K. At 500 K, the apparent thermal conductivity is reduced from 21.5 W/mK to 18 W/mK in 0.8–10 MHz frequency range. The trend is consistent with Refs. 6 and 25. However, at low temperature, e.g., 100 K, the main contribution to thermal conductivity comes from long mean-free-path phonons, which may be scattered by the $Al_{0.1}Ga_{0.9}N$/GaN interface.[26] Therefore, the apparent thermal conductivity is independent of the modulation frequency at these low temperatures. At intermediate temperatures, 150–200 K, the apparent thermal conductivity is constant in the modulation frequency range of 0.8–6 MHz and then drops around 10% in 6–10 MHz range. We believe that

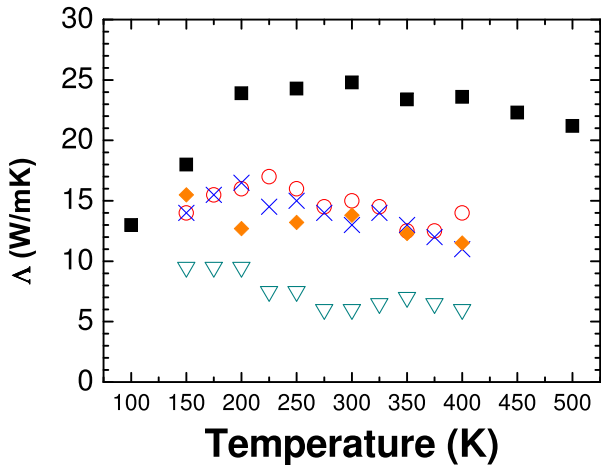

FIG. 3. Thermal conductivity of 1.2 μm (■) and 0.2 μm (◆) $Al_{0.1}Ga_{0.9}N$ thin film versus temperature. As plotted are the measurements of $Al_{0.18}Ga_{0.82}N$ (x), $Al_{0.2}Ga_{0.8}N$ (○), and $Al_{0.44}Ga_{0.56}N$ (Δ) thermal conductivity reported in Ref. 2.

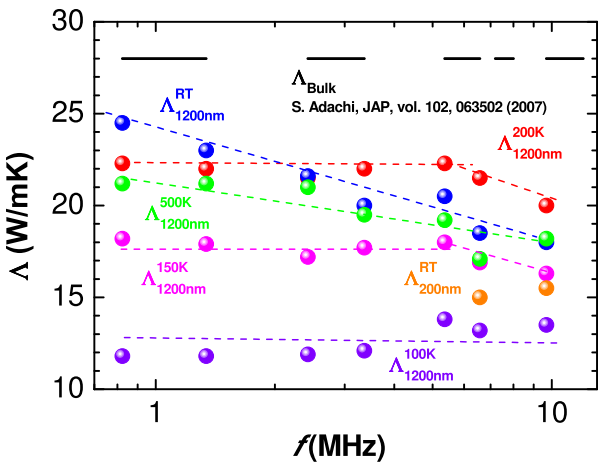

FIG. 4. Thermal conductivity of 1.2 μm $Al_{0.1}Ga_{0.9}N$ sample versus pump modulation frequencies at 100–500 K.

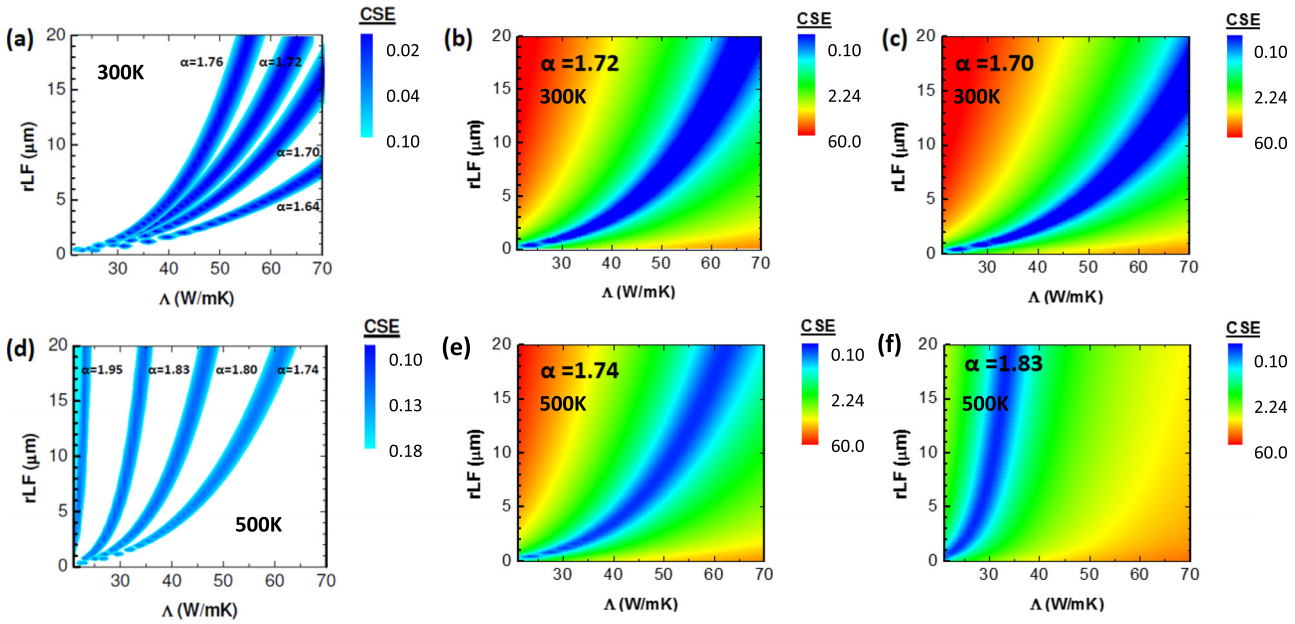

FIG. 5. Cumulative square error (CSE) fitting experimental TDTR data with the Tempered Lévy model as a function of r_{LF} and thermal conductivity Λ, for different fractal dimension α values at 300 K ((a)–(c)) and 500 K ((d)–(f)). Figures (a) and (d) show the minimum CSE region for different α values. The αs used in (b) and (e) are based on first-principles calculations reported in Ref. 27, while αs used in (c) and (f) are based on the optimum fitting of the TDTR data with the Tempered Lévy model.

150–200 K measurements show the transition from dominant boundary scattering to alloy scattering at 6 MHz.

Tempered Lévy analysis of the raw TDTR signals produced superdiffusion exponents $\alpha = 1.70 \pm 0.06$ at 300 K and $\alpha = 1.83 \pm 0.16$ at 500 K, comparable to the respective values of 1.72 and 1.74 obtained from first-principles calculations.[27] Beyond interface thermal resistance, three parameters: fractal dimension α, Lévy-Fourier transition length r_{LF}, and bulk thermal conductivity Λ are needed to describe the full TDTR data of any material at all frequencies. Figures 5(a)–5(f) show the cumulative square error fitting experimental TDTR data with Tempered Lévy model as a function of r_{LF} and thermal conductivity Λ with different α at 300 K and 500 K. The curved blue bands (minimum error) in the error maps indicate a strong correlation between rLF and thermal conductivity. Closer inspection shows that the bands constitute regions of constant fractional diffusivity $(\Lambda/C)/{r_{LF}}^{2-\alpha} = D_\alpha$. So even though the available data are insufficient for a full extraction of all individual parameters, the tempered Lévy analysis still leads to a self-consistent and unambiguous identification of the sample's superdiffusive heat conduction properties. If we assume the bulk thermal conductivity at 300 K is between 24.5 W/mK (Figure 4, Fourier analysis) to 38.7 W/mK (*ab-initio*, c-axis),[25] Fig. 5 shows that r_{LF} should be 1–3 μm at 300 K and 0.5–2 μm at 500 K. The above correlation shows that the experimental data are limited and using high-frequency data ($f > 9$ MHz) to analyze the response of the 1.2 μm thick film is not sufficient to fully characterize quasi-ballistic heat transport in $Al_{0.1}Ga_{0.9}N$. A thicker $Al_{0.1}Ga_{0.9}N$ film is needed to be able to do TDTR at lower frequencies and capture accurate r_{LF} and thermal conductivity values. Alternatively, a multi-layer Tempered Lévy model will be extremely helpful to fully analyze low frequency TDTR data taking into account ballistic effects both in the thin film and in the substrate. Such a model does not currently exist, but this should be a good topic for future studies.

Thermal conductivity of 1.2 μm thick $Al_{0.1}Ga_{0.9}N$ layers grown using PAMBE was measured in 0.8–10 MHz modulation frequency range with an ultrafast pump and probe TDTR technique. The phonon ballistic effect for $Al_xGa_{1-x}N$ has been observed. Temperature dependent measurements in 100–500 K temperature range show rich frequency-dependent thermal conductivity indicating the interplay between phonon boundary scattering at the interface between the thin film and substrate and the Umklapp scattering inside the film. Tempered Lévy analysis is used to extract the fractal dimension of the superdiffusive transport at short time and length scales. A Lévy fractal dimension of $\alpha \approx 1.70 \pm 0.06$ at room temperature, and $\alpha \approx 1.83 \pm 0.16$ at 500 K can be extracted showing that the thermal transport is within the quasi-ballistic regime.

See supplementary material for short descriptions on the time-domain thermoreflectance (TDTR) measurement system, heat transfer model (3D thermal diffusion model based on thermal quadrupole), and Tempered Lévy theory.

This work was partially supported by the National Science Foundation (Award No. DMR-1206919). The authors would like to thank Dr. Bivas Saha and Dr. Amirkoushyar Ziabari for useful discussion.

[1]H. Morkoc, *Nitride Semiconductor and Devices* (Springer, Heidelberg, 1999).
[2]B. C. Daly, H. J. Maris, A. V. Nurmikko, M. Kuball, and J. Han, J. Appl. Phys. **92**, 3820 (2002).
[3]S. Adachi, J. Appl. Phys. **102**, 063502 (2007).
[4]B. Abeles, Phys Rev. **131**, 1906 (1963).
[5]V. Palankovski, R. Schultheis, and S. Selberherr, IEEE Trans. Electron Devices **48**, 1264–1269 (2001).
[6]Y. K. Koh and D. G. Cahill, Phys. Rev. B **76**, 075207 (2007).

[7]B. Vermeersch, A. M. S. Mohammed, G. Pernot, Y. R. Koh, and A. Shakouri, Phys. Rev. B **91**, 085203 (2015).
[8]B. Vermeersch, J. Carrete, N. Mingo, and A. Shakouri, Phys. Rev. B **91**, 085202 (2015).
[9]B. Vermeersch, A. M. S. Mohammed, G. Pernot, Y. R. Koh, and A. Shakouri, Phys. Rev. B **90**, 014306 (2014).
[10]D. G. Cahill, Rev. Sci. Instrum. **75**, 5119 (2004).
[11]S. Dilhaire, G. Pernot, G. Calbris, J. M. Rampnoux, and S. Grauby, J. Appl. Phys. **110**, 114314 (2011).
[12]A. J. Schmidt, X. Chen, and G. Chen, Rev. Sci. Instrum. **79**, 114902 (2008).
[13]B. Vermeersch, G. Pernot, Y. R. Koh, P. Abumov, and A. Shakouri, in *Proceedings of the 13th InterSociety Conference on Thermal and Thermomechanical Phenomena in Electronic Systems, ITherm* (2012), pp. 428–434.
[14]E. D. Palik, *Handbook of Optical Constants of Solids* (Academic Press, Orlando, 1985).
[15]Y. Wang, J. Y. Park, Y. K. Koh, and D. G. Cahill, J. Appl. Phys. **108**, 043507 (2010).
[16]S. Dilhaire, J. M. Rampnoux, S. Grauby, G. Pernot, and G. Calbris, in *ASME 2009 Second International Conference on Micro/Nanoscale Heat and Mass Transfer* (2009), Vol. 2, pp. 451–456.
[17]Y. K. Koh, S. L. Singer, W. Kim, J. M. O. Zide, H. Lu, D. G. Cahill, A. Majumdar, and A. C. Gossard, J. Appl. Phys. **105**, 054303 (2009).
[18]B. Vermeersh, J. Appl. Phys. **120**, 175102 (2016).
[19]A. M. S. Mohammed, Y. R. Koh, B. Vermeersch, H. Lu, P. G. Burke, A. C. Gossard, and A. Shakouri, Nano Lett. **15**(7), pp. 4269–4273 (2015).
[20]W. Liu and A. A. Balandin, Appl. Phys. Lett. **85**(22), 5230–5232 (2004).
[21]W. Liu and A. A. Balandin, J. Appl. Phys. **97**, 073710 (2005).
[22]T. S. Fisher, *Thermal Energy at the Nanoscale* (World Scientific, Singapore, 2014).
[23]P. G. Klemens, Phys. Rev. **119**, 507 (1960).
[24]P. G. Klemens, Int. J. Thermophys. **22**, 265 (2001).
[25]K. T. Regner, D. P. Sellan, Z. Su, C. H. Amon, A. J. H. McGaughey, and J. A. Malen, Nat. Commun. **4**, 1640 (2013).
[26]P. G. Klemens, Solid State Phys. Adv. Res. Appl. **7**, 1–98 (1958).
[27]B. Vermeersch, J. Carrete, and N. Mingo, Appl. Phys. Lett. **108**, 193104 (2016).